ADVANCED OPTICAL MATERIALS
www.advopticalmat.de

Compelling Evidence for the ε-Phase InSe Crystal by Oblique Incident Second Harmonic Generation

Zeyuan Sun, Yu Zhang, Jimin Qian, Ruixi Qiao, Xian Li, Zerui Wang, Changlin Zheng, Kaihui Liu, Ting Cao, Wei-Tao Liu, and Shiwei Wu**

Indium selenide (InSe), a layered semiconductor with direct band gap and high carrier mobility, holds promising applications in bendable electronics and ultrafast optoelectronics. Yet its crystal structure exhibits polytypism with four different stacking orders (γ-, ε-, β- and δ-phases), arising from the weak van der Waals interlayer coupling. These phases are nearly-degenerate in energy but are predicted to have contrasting electronic structures for versatile applications. It remains highly challenging to distinguish between these polytypes due to the lack of noninvasive tools that are sensitive enough to the interlayer structural variations. Here, the unambiguous discrimination of different InSe polytypes using symmetry-sensitive oblique incident optical second harmonic generation (SHG) is demonstrated. Surprisingly, the ε-phase is found to be dominant, although the samples from two popular commercial vendors (2D Semiconductors and Six Carbon Technology) are claimed to be the γ-phase. These results would help promoting the precise application of InSe crystal for piezoelectric transducer and strain sensing, as well as showing the oblique incident SHG to be a powerful structural analytical tool for van der Waals layered materials.

1. Introduction

The stacking order of layered van der Waals materials plays a key role in the engineering of electronic and optical properties. For example, in transition metal dichalcogenides (TMDCs) such as MoS_2, the stacking order controls the bandgap energy and determines the spin-valley coupling.[1,2] For trilayer graphene, the electronic structures of ABA- and ABC-stacking are totally different: the ABA-stacking is a semimetal and ABC-stacking is a semiconductor upon applying an electric field.[3–5] The unambiguous determination of the interlayer stacking order is therefore crucial for understanding and utilizing van der Waals materials. Recently, indium selenide (InSe) has attracted much attention as a highly promising candidate for bendable electronics and ultrafast optoelectronics.[6–8] It belongs to the family of III-VI metal monochalcogenide semiconductors including GaS and GaSe, exhibiting high carrier mobility and direct bandgap from bulk to thin flakes. Prototype InSe-based devices such as bendable photodetectors,[7] p-n junctions,[9] and field-effect-transistors[10] showed better performance than those based on graphene and TMDCs.

Nonetheless, stacking order, the basic structural property of InSe, remains largely controversial. The monolayer InSe

Z. Sun, Y. Zhang, X. Li, Z. Wang, C. Zheng, W.-T. Liu, S. Wu
State Key Laboratory of Surface Physics
Key Laboratory of Micro and Nano Photonic Structures (MOE)
and Department of Physics
Fudan University
Shanghai 200433, China
E-mail: wtliu@fudan.edu.cn; swwu@fudan.edu.cn

J. Qian, T. Cao
Department of Materials Science and Engineering
University of Washington
Seattle, Washington 98195, USA

R. Qiao, K. Liu
State Key Lab for Mesoscopic Physics and Frontiers Science Center
for Nano-optoelectronics
Collaborative Innovation Center of Quantum Matter
School of Physics
Peking University
Beijing 100871, China

S. Wu
Shanghai Qi Zhi Institute
Shanghai 200232, China

S. Wu
Institute for Nanoelectronic Devices and Quantum Computing
and Zhangjiang Fudan International Innovation Center
Fudan University
Shanghai 200433, China

S. Wu
Shanghai Research Center for Quantum Sciences
Shanghai 201315, China

The ORCID identification number(s) for the author(s) of this article can be found under https://doi.org/10.1002/adom.202201183.

DOI: 10.1002/adom.202201183

consists of covalently bonded Se-In-In-Se atomic planes and has a honeycomb structure viewed from the top[6] (**Figure 1**a). The bulk InSe has four polytypes named γ-, ε-, β- and δ-phases[7,8,10,11]

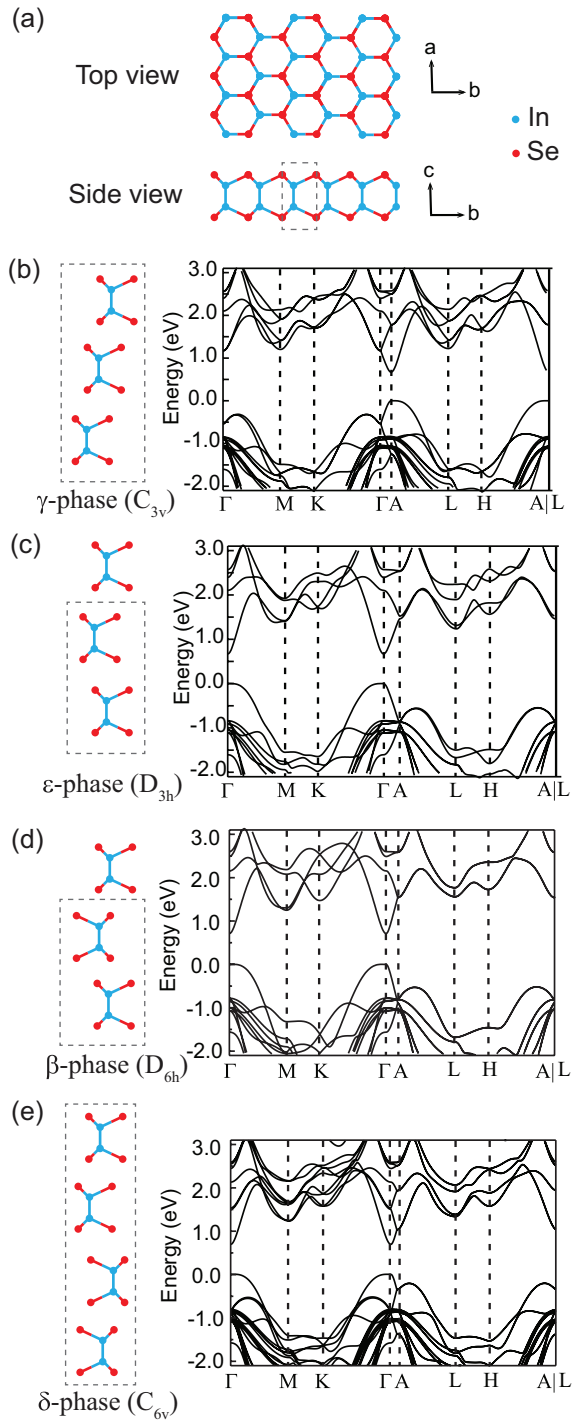

Figure 1. Stacking order and electronic structure of different InSe phases. a) Top and side view of monolayer InSe. The indium and selenium atoms are illustrated by blue and red spheres, respectively. b–e) Side view of γ-, ε-, β- and δ-phases of InSe crystals, respectively. The corresponding Kohn-Sham band structures calculated within the PBE functional are shown on their right. The dashed boxes show the conventional cell in each phase.

(Figure 1b–e, left panels), depending on the configurations of van der Waals stacking. Theoretical calculations showed that these polytypes have considerably different electronic structures,[12] as shown in Figure 1b–e (right panels). For example, in contrast to other three phases, the γ-phase is expected to have multiple degenerate energy valleys at A points (Figure 1b). Based on the density functional theory calculations within the PBE-D2 formalism, γ-phase is the most stable phase among the four polytypes under ambient conditions, but is favorable by only a fraction of meV per In_2Se_2 unit (see details in Supporting Information). Previous studies have characterized the InSe structure with X-ray diffraction (XRD),[7,10] transmission electron microscopy (TEM),[13,14] and Raman spectra.[7,13] Though many studies considered the γ-phase to be the most widely existing and stable form,[6,8] some also indicated the existence of ε-[7,15] or β-phase,[10] or coexistence of γ- and ε-phase.[13]

To resolve the exact polytype of InSe, techniques that are sensitive to the subtle change between different stacking orders are required. Because the four polytypes of InSe belong to different point groups and are characterized by distinct crystallographic symmetries, a symmetry-specific characterization tool would be ideal to resolve the above controversies. Here we report an oblique incident second harmonic generation (SHG) study for resolving different polytypes of InSe. SHG is well known as a second-order nonlinear optical process and has emerged as a powerful and noninvasive tool to characterize van der Waals materials.[2,5,16–22] The basic principles of SHG was described elsewhere.[23,24] Briefly, the SHG intensity can be written as: $I(2\omega) \propto |\overleftrightarrow{\chi}^{(2)} : \mathbf{E}(\omega)\mathbf{E}(\omega)|^2$, where $\mathbf{E}(\omega)$ is the electric field of the fundamental input at frequency ω, and $\overleftrightarrow{\chi}^{(2)}$ is the corresponding nonlinear optical susceptibility tensor. As a third-rank tensor, $\overleftrightarrow{\chi}^{(2)}$ is highly sensitive to various symmetry properties of the materials, including the stacking orders of layered van der Waals compounds, such as the trilayer graphene, few-layer TMDCs, and transition metal monochalcogenides.[2,5,19,20,25] Previous SHG studies on InSe have revealed its high second-order optical nonlinearities.[14,15,26] However, they were done with the commonly adopted normal incident geometry, which was not sensitive to out-of-plane $\overleftrightarrow{\chi}^{(2)}$ elements. By utilizing an oblique incident geometry, we are now able to detect the out-of-plane components that are essential for differentiating various InSe polytypes (details discussed below), and show the ε-phase to be dominant, instead of the commonly proposed γ-phase. Corroborated by selected area electron diffraction patterns from TEM measurement, the result would serve to guide future studies on InSe and related applications such as piezoelectric transducer and strain sensing.[7,27–29]

2. Results and Discussion

The γ-, ε-, β- and δ-phases of InSe belong to the point groups of C_{3v}, D_{3h}, D_{6h}, and C_{6v},[11] respectively (Figure 1b–e, left panels). Among them, the D_{6h} group has inversion symmetry, hence SHG from the β-phase InSe is forbidden under electric dipole approximation.[23,24] Regarding the ε-phase of the D_{3h} point group, it has an out-of-plane three-fold rotational axis, and mirror planes both parallel and perpendicular

to the three-fold axis. These symmetries lead to nonzero $\overleftrightarrow{\chi}^{(2)}$ tensor elements as: $\chi^{(2)}_{bbb,\varepsilon} = -\chi^{(2)}_{baa,\varepsilon} = -\chi^{(2)}_{aab,\varepsilon} = -\chi^{(2)}_{aba,\varepsilon}$. Here a and b refer to the in-plane lattice coordinates defined in Figure 1a, with a along the zigzag direction and b along the arm-chair direction. For the γ-phase of C_{3v} symmetry, the corresponding $\overleftrightarrow{\chi}^{(2)}$ contains the same set of in-plane elements $\chi^{(2)}_{bbb,\gamma} = -\chi^{(2)}_{baa,\gamma} = -\chi^{(2)}_{aab,\gamma} = -\chi^{(2)}_{aba,\gamma}$; in addition, it also contains a set of nonzero elements involving the c-axis along surface normal, which are $\chi^{(2)}_{aca,\gamma} = \chi^{(2)}_{bcb,\gamma} = \chi^{(2)}_{aac,\gamma} = \chi^{(2)}_{bbc,\gamma}$, $\chi^{(2)}_{caa,\gamma} = \chi^{(2)}_{cbb,\gamma}$, and $\chi^{(2)}_{ccc,\gamma}$. Here, the major distinction between ε- and γ-phases lies in the set of out-of-plane tensor elements, arising from the reduced symmetry of γ-phase. For the δ-phases with C_{6v} point group, all the nonzero $\overleftrightarrow{\chi}^{(2)}$ tensor elements involve the c-axis along surface normal, which are $\chi^{(2)}_{aca,\delta} = \chi^{(2)}_{bcb,\delta} = \chi^{(2)}_{aac,\delta} = \chi^{(2)}_{bbc,\delta}$, $\chi^{(2)}_{caa,\delta} = \chi^{(2)}_{cbb,\delta}$, and $\chi^{(2)}_{ccc,\delta}$. It is seen that the isotropic response (originated from out-of-plane components) is the key to distinguish different phases, which is not detectable via the normal incidence usually adopted. Hence the oblique incident geometry must be utilized.[23,24]

Our InSe single crystals were purchased from 2D Semiconductors and Six Carbon Technology, both labeled as γ-phase by their specification. The samples from 2D Semiconductors were mechanically exfoliated on PDMS and dry transferred to the oxide-covered silicon substrate. The sample thickness was about 90 nm determined by atomic force microscopy. Figure S1a,b, Supporting Information, shows the photoluminescence and Raman spectra of the samples. The photoluminescence spectrum exhibited a peak at 998 nm, and the Raman spectrum showed major peaks at 115.3, 117.3, and 227.5 cm^{-1}, corresponding to A^1_{1g}, E^1_{2g} and A^2_{1g} phonon modes reported by previous studies.[6,13] It is noted that a weak shoulder at 193 cm^{-1} was also detected, which corresponded to the E^2_{2g} mode, and was often considered to be indicating the ε-phase.[30] Yet there remained controversy on the Raman spectra analysis, so we could not determine the polytype phase based on this mode alone[7,31,32] (see details in Supporting Information).

In SHG measurements, we adopted the oblique incident geometry to excite and acquire electric field components along the c-axis, as sketched in **Figure 2**a. The excitation beam was incident at ≈45° from the surface normal.[33] The SHG signal at 2ω from InSe samples was detected along the direction of specular reflection. By rotating the samples around the surface normal, we collected the SHG anisotropic patterns versus the azimuthal angle φ, which is the angle between a-axis (zigzag direction) and incident plane (see inset of Figure 2a). So at $\varphi = 0$, the zigzag direction lies in the beam incident plane. At different input and output polarization combinations, for the ε-phase, the SHG anisotropic patterns are described by: $I_{SSS,\varepsilon}(\varphi) \propto I_{SPP,\varepsilon}(\varphi) \propto |\chi^{(2)}_{bbb,\varepsilon}\cos(3\varphi)|^2$, and $I_{PSS,\varepsilon}(\varphi) \propto I_{PPP,\varepsilon}(\varphi) \propto |\chi^{(2)}_{bbb,\varepsilon}\cos(3\varphi)|^2$ (see details of derivation in Supporting Information). Here, the first letter in the subscript of $\overleftrightarrow{\chi}^{(2)}$ refers to the polarization of the output beam, and the other

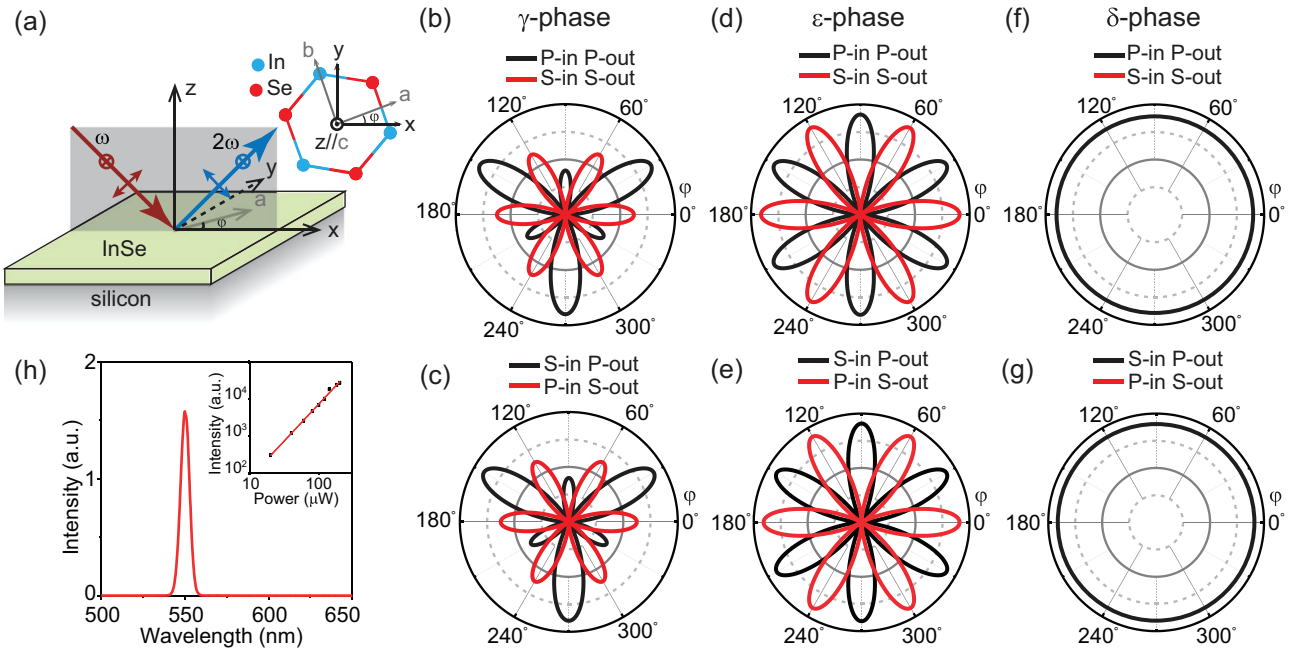

Figure 2. Simulated SHG of γ-, ε- and δ-phase InSe under oblique incidence. a) Schematic of the experimental geometry at oblique incidence of ≈45°. Polarizations of the fundamental and second harmonic beams are denoted by double-headed arrows (P-polarization) and cross-inside circles (S-polarization). The inset is the schematic of the crystal coordinate (a-b-c) and the laboratory coordinate (x-y-z). The azimuthal angle φ between the x-axis and the a-axis is illustrated. b,c) Simulated SHG polarization patterns of γ-phase InSe with different polarization combinations. The SHG patterns become asymmetric when P-polarized SHG signals are selected. In the simulation, the isotropic term was set to five times smaller than the anisotropic term. d,e) Corresponding simulation results for ε-phase InSe. Different from γ-phase InSe, all the SHG polarization patterns are six-fold symmetric. f,g) Corresponding simulation results for δ-phase InSe. Different from γ- and ε-phase InSe, the S-polarized SHG signals vanish and the P-polarized SHG signals are isotropic. h) Strong SHG at 550 nm from an InSe flake (90 nm thick). The excitation wavelength was 1100 nm and incident power was about 1 mW. The inset is the power dependence of the SHG intensities on a double-logarithmic scale. Solid line is the fit with a slope of 2.0 ± 0.03.

two refer to the polarization of the input beam. For example, "*SSS*" refers to the polarization combination with S-polarized output and S-polarized input (Figure 2a), "*SPP*" refers to the case with S-polarized output and P-polarized input, and so on. For the γ-phase, the *SSS* and *SPP* terms have the same forms as those of the ε-phase, that are: $I_{SSS,\gamma}(\varphi) \propto I_{SPP,\gamma}(\varphi) \propto |\chi^{(2)}_{bbb,\gamma}\cos(3\varphi)|^2$. However, the *PSS* and *PPP* patterns of the γ-phase are both different from those of the ε-phase, with additional isotropic terms that are independent of φ. We have: $I_{PSS,\gamma}(\varphi) \propto |\chi^{(2)}_{bbb,\gamma}\sin(3\varphi) + iso_{PSS,\gamma}|^2$ and $I_{PPP,\gamma}(\varphi) \propto |\chi^{(2)}_{bbb,\gamma}\sin(3\varphi) + iso_{PPP,\gamma}|^2$, with $iso_{PSS,\gamma} \propto \chi^{(2)}_{cbb,\gamma}$, $iso_{PPP,\gamma}$ being a function of $\chi^{(2)}_{cbb,\gamma}$, $\chi^{(2)}_{bbc,\gamma}$ and $\chi^{(2)}_{ccc,\gamma}$ (see details of derivation in Supporting Information). Here, tensor elements contributing to the isotropic terms all involve transition dipole moments along the *c*-axis. Interestingly, for the δ-phase, all anisotropic terms now vanish, and only the isotropic terms remain. So we only have $I_{PSS,\delta}$ and $I_{PPP,\delta}$ being detectable, which are both independent of φ.

Figure 2 presents simulated SHG patterns with different polarization combinations for the γ-phase (Figure 2b,c), ε-phase (Figure 2d,e), and δ-phase (Figure 2f,g), all normalized with respect to the maximum intensity for easy comparison. For the ε-phase, all SHG patterns are six-fold symmetric regardless of the polarization combination. For the γ-phase, both SSS and SPP patterns are six-fold, while the PSS and PPP patterns are three-fold due to the interference between anisotropic and isotropic terms. For the δ-phase, all patterns are isotropic. Therefore, the ε-, γ- and δ-phase InSe can be readily distinguished via the PSS and PPP patterns.

Figure 2h shows the emission spectra of the InSe samples excited by a 200 fs, 80 MHz pulsed laser at 1100 nm, showing the SHG peak at half of the input wavelength. The excitation wavelength was chosen for a strong SHG response (see Figure S1c, Supporting Information, for the SHG excitation spectrum). The inset plots the SHG intensity versus the excitation power in the double logarithmic scale, showing a quadratic power law dependence (2.0 ± 0.03) as expected. This strong SHG response immediately excludes the centrosymmetric β-phase that could not produce SHG under the electric dipole approximation. We then acquired the azimuthal anisotropic patterns to distinguish between the ε-, γ- and δ-phase by rotating the sample around its surface normal. **Figure 3**a,b displays the measured patterns, which all exhibited six-fold rotational symmetry, regardless of the input and output polarizations. The isotropic component specific to the γ- and δ-phases was absent in all cases. Such six-fold SHG patterns strongly suggested that the InSe samples

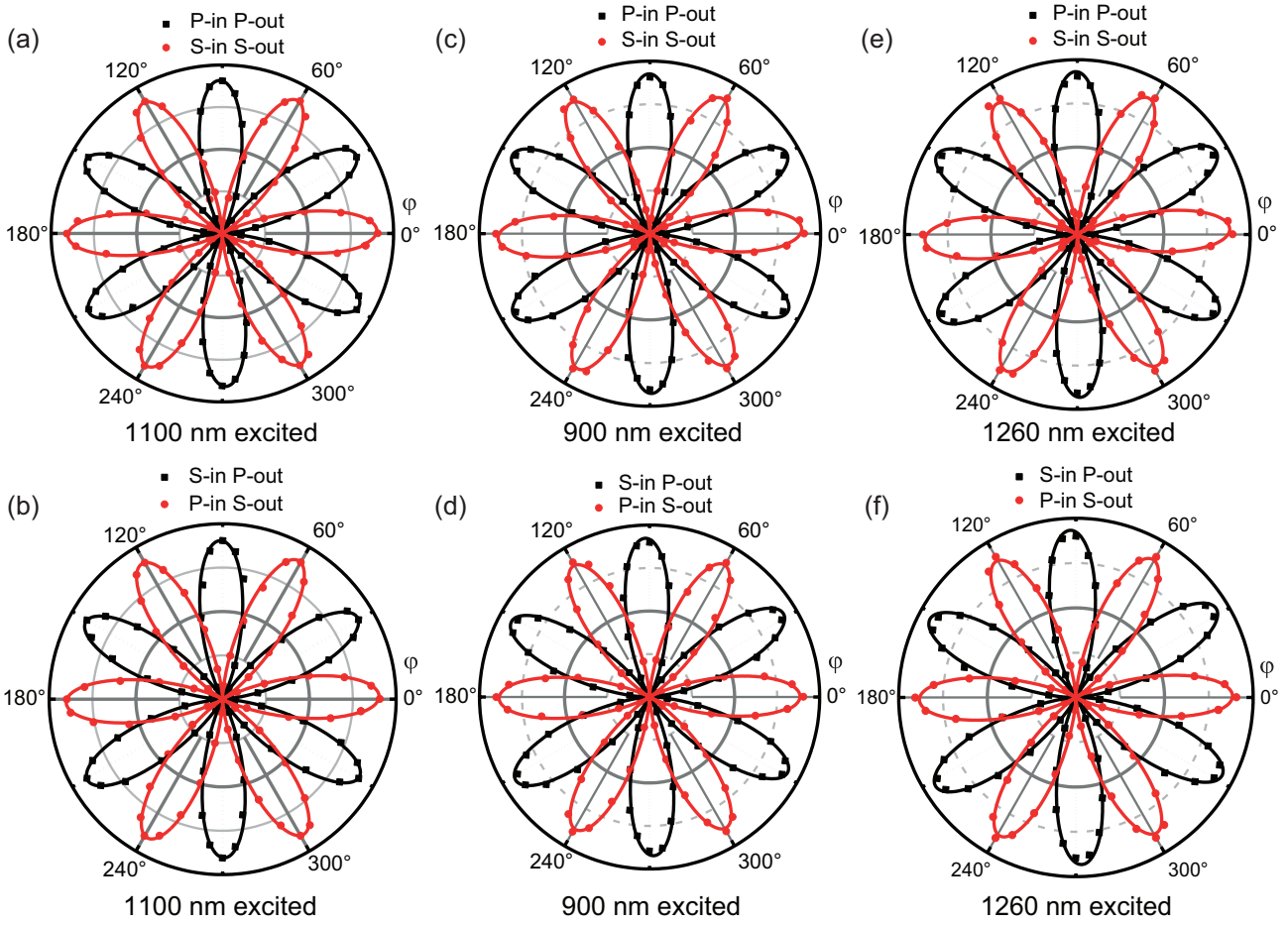

Figure 3. Azimuthal SHG polarization-resolved patterns of the InSe at different fundamental wavelength under oblique incidence: a,b) for the fundamental wavelength at 1100 nm, c,d) for 900 nm, and e,f) for 1260 nm. All the polarization-resolved patterns display six-fold symmetry, independent of the fundamental beam wavelength, suggesting the ε-phase InSe.

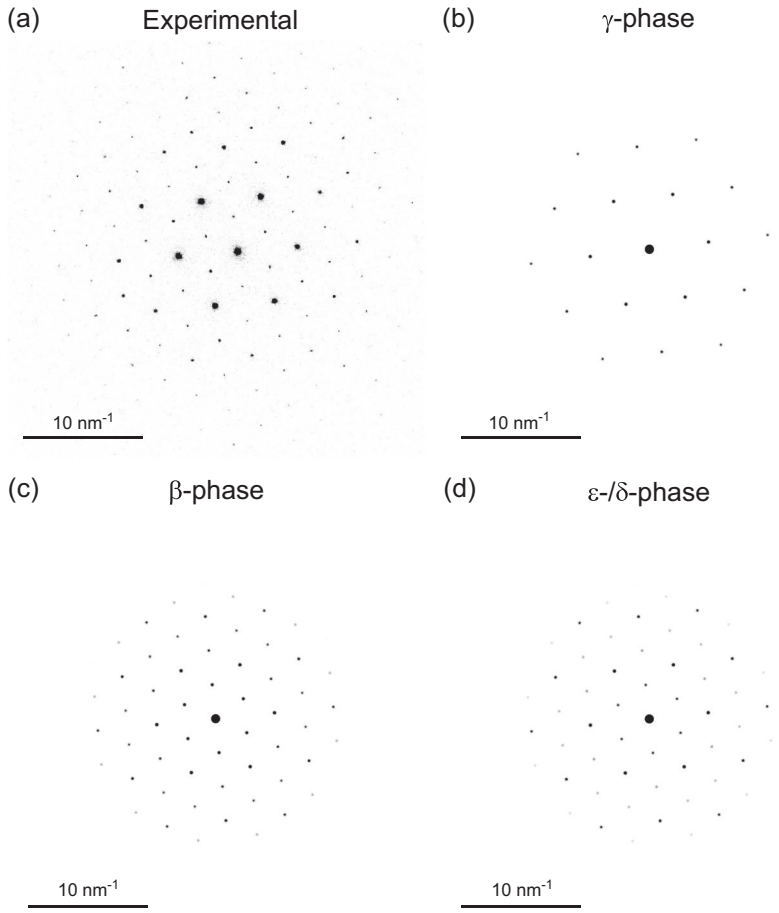

Figure 4. TEM study of InSe flakes. a) SAED pattern of the InSe sample (about 20 nm thick). b–d) Simulated electron diffraction patterns of the γ-, β- and ε-/δ-phase InSe crystals, respectively. Note that the ε- and δ-phases share the same SAED pattern, as shown in (d). By comparison, the measured pattern in (a) matches with that from ε- and δ-phases shown in (d).

were dominated by the ε-phase, rather than the more commonly proposed γ-phase.

It might still be argued that even for the γ-phase and δ-phase, the isotropic components could be vanishing if related transition dipole moments along the *c*-axis happened to be small. While due to the nature of their point groups, such accidental cancellation would only happen to specific resonances, but cannot be a general property at all other wavelength. To check that, we tuned the excitation wavelength to 900 nm and 1260 nm, which are above and below the resonance on the excitation spectrum, respectively (Figure S1c, Supporting Information). Again, all SHG patterns exhibited the six-fold symmetry characteristic for the ε-phase, without any trace of isotropic contribution from the γ-phase or δ-phase (Figure 3). We further checked the samples of various thicknesses to avoid the accidental segregation of various phases, and the six-fold patterns persisted (Figure S2, Supporting Information), showing that the ε-phase dominates the entire crystal. We also tested InSe samples purchased from a different vendor (Six Carbon Technology), which was also claimed to be the γ-phase. Again, our measurement revealed the ε-phase to be dominant, as shown in Figure S3, Supporting Information.

To corroborate the result, we further performed a detailed TEM measurement on InSe thin flakes. **Figure 4**a shows the selected area electron diffraction (SAED) pattern of the InSe sample, which was composed of both primary and secondary sets of hexagonal patterns. Figures 4b–d display the simulated electron diffraction patterns of γ-, β- and ε-/δ-phases, respectively. For the β-phase, the intensity of the primary set is equal to that of the second set. For the γ-phase, the primary set of diffraction spots is completely absent due to destructive interference. The ε- and δ-phases share the same SAED pattern, showing contrasting intensity between the primary and secondary sets (Figure 4d). Therefore, the TEM result in Figure 4a also excludes the γ-phase and β-phase as SHG. As the six-fold SHG anisotropy patterns further exclude the δ-phase, the dominance of ε-phase in InSe crystal becomes unambiguous.

3. Conclusion

In summary, we identified the stacking order of InSe to be the ε-phase using oblique incident SHG under ambient conditions. The result was further corroborated by TEM measurements, and

is in accordance with theoretical simulations. This identification can serve as a base for further exploring the physical properties of InSe as well as the device applications such as piezoelectric transducer and strain sensing.[7,27–29] Our work also demonstrates that the symmetry-sensitive SHG technique is a powerful noninvasive method for crystallographic structure analysis, which can be widely applied to other van der Waals layered materials.

4. Experimental Section

Optical Measurement: The SHG polarization-resolved patterns were conducted on an optical microscopic system at oblique incidence.[33] In this setup, a femtosecond optical parametric oscillator (OPO, 200 fs pulse duration, 80 MHz repetition rate) with tunable wavelength was used as the excitation source. The linearly polarized light was focused onto the sample at ≈45° angle by 10× long working-distance objective (NA = 0.3). The reflected SHG signal was collected by a 50× long working-distance objective (NA = 0.4), and guided to a fiber-coupled spectrograph equipped with a liquid nitrogen-cooled silicon charge-coupled device to acquire optical spectra. The InSe SHG excitation spectroscopy measurement (Figure S1c, Supporting Information) was conducted on an optical microscope at normal incidence. In this setup, the fundamental beam was linearly polarized and tunable from 800 to 1300 nm, and focused on the sample by a 100× microscopic objective (NA = 0.95). The reflected SHG signal was collected by the sample objective and guided to a fiber coupled spectrograph equipped with a liquid nitrogen-cooled silicon charge-coupled device. The photoluminescence and Raman measurements were conducted on the same optical microscope at normal incidence. The photoluminescence signal was detected by a liquid nitrogen cooled InGaAs charge-coupled device.

TEM Measurements and Analysis: SAED patterns were acquired at an aberration-corrected transmission electron microscope (FEI Titan Themis G2 300) operated at 300 kV. The simulations of the SAED pattern were performed using Crystalmaker software.

Supporting Information

Supporting Information is available from the Wiley Online Library or from the author.

Acknowledgements

Z.S. and Y.Z. contributed equally to this work. The work at Fudan University was supported by the National Key Research and Development Program of China (Grant Nos. 2019YFA0308404), National Natural Science Foundation of China (Grant Nos. 12034003, 91950201, 11991062, 12004077), Science and Technology Commission of Shanghai Municipality (Grant No. 20JC1415900, 2019SHZDZX01, 21JC1402000), Program of Shanghai Academic Research Leader (Grant No. 20XD1400300), and China National Postdoctoral Program for Innovative Talents (Grant No. BX20200086). K.L. was supported by the Strategic Priority Research Program of the Chinese Academy of Sciences (XDB33000000).

Conflict of Interest

The authors declare no conflict of interest.

Data Availability Statement

The data that support the findings of this study are available from the corresponding author upon reasonable request.

Keywords

InSe, polytypes, second harmonic generation, stacking order

Received: June 7, 2022
Published online:

[1] Q. H. Wang, K. Kalantar-Zadeh, A. Kis, J. N. Coleman, M. S. Strano, *Nat. Nanotechnol.* **2012**, *7*, 699.
[2] T. Jiang, H. Liu, D. Huang, S. Zhang, Y. Li, X. Gong, Y. R. Shen, W. T. Liu, S. Wu, *Nat. Nanotechnol.* **2014**, *9*, 825.
[3] W. Bao, L. Jing, J. Velasco, Y. Lee, G. Liu, D. Tran, B. Standley, M. Aykol, S. B. Cronin, D. Smirnov, M. Koshino, E. McCann, M. Bockrath, C. N. Lau, *Nat. Phys.* **2011**, *7*, 948.
[4] C. H. Lui, Z. Li, K. F. Mak, E. Cappelluti, T. F. Heinz, *Nat. Phys.* **2011**, *7*, 944.
[5] Y. Shan, Y. Li, D. Huang, Q. Tong, W. Yao, W. T. Liu, S. Wu, *Sci. Adv.* **2018**, *4*, eaat0074.
[6] G. W. Mudd, S. A. Svatek, T. Ren, A. Patane, O. Makarovsky, L. Eaves, P. H. Beton, Z. D. Kovalyuk, G. V. Lashkarev, Z. R. Kudrynskyi, A. I. Dmitriev, *Adv. Mater.* **2013**, *25*, 5714.
[7] S. R. Tamalampudi, Y. Y. Lu, U. R. Kumar, R. Sankar, C. D. Liao, B. K. Moorthy, C. H. Cheng, F. C. Chou, Y. T. Chen, *Nano Lett.* **2014**, *14*, 2800.
[8] D. A. Bandurin, A. V. Tyurnina, G. L. Yu, A. Mishchenko, V. Zolyomi, S. V. Morozov, R. K. Kumar, R. V. Gorbachev, Z. R. Kudrynskyi, S. Pezzini, Z. D. Kovalyuk, U. Zeitler, K. S. Novoselov, A. Patane, L. Eaves, I. V. Grigorieva, V. I. Fal'ko, A. K. Geim, Y. Cao, *Nat. Nanotechnol.* **2017**, *12*, 223.
[9] N. Balakrishnan, Z. R. Kudrynskyi, M. W. Fay, G. W. Mudd, S. A. Svatek, O. Makarovsky, Z. D. Kovalyuk, L. Eaves, P. H. Beton, A. Patanè, *Adv. Opt. Mater.* **2014**, *2*, 1064.
[10] W. Feng, W. Zheng, W. Cao, P. Hu, *Adv. Mater.* **2014**, *26*, 6587.
[11] D. T. Do, S. D. Mahanti, C. W. Lai, *Sci. Rep.* **2015**, *5*, 17044.
[12] J. Srour, M. Badawi, F. El Haj Hassan, A. Postnikov, *J. Chem. Phys.* **2018**, *149*, 054106.
[13] S. Lei, L. Ge, S. Najmaei, A. George, R. Kappera, J. Lou, M. Chhowalla, H. Yamaguchi, G. Gupta, R. Vajtai, A. D. Mohite, P. M. Ajayan, *ACS Nano* **2014**, *8*, 1263.
[14] J. Zhou, J. Shi, Q. Zeng, Y. Chen, L. Niu, F. Liu, T. Yu, K. Suenaga, X. Liu, J. Lin, Z. Liu, *2D Mater.* **2018**, *5*, 025019.
[15] Q. Hao, H. Yi, H. Su, B. Wei, Z. Wang, Z. Lao, Y. Chai, Z. Wang, C. Jin, J. Dai, W. Zhang, *Nano Lett.* **2019**, *19*, 2634.
[16] Y. Li, Y. Rao, K. F. Mak, Y. You, S. Wang, C. R. Dean, T. F. Heinz, *Nano Lett.* **2013**, *13*, 3329.
[17] N. Kumar, S. Najmaei, Q. Cui, F. Ceballos, P. M. Ajayan, J. Lou, H. Zhao, *Phys. Rev. B* **2013**, *87*, 161403.
[18] H. Zeng, G. B. Liu, J. Dai, Y. Yan, B. Zhu, R. He, L. Xie, S. Xu, X. Chen, W. Yao, X. Cui, *Sci. Rep.* **2013**, *3*, 1608.
[19] W. T. Hsu, Z. A. Zhao, L. J. Li, C. H. Chen, M. H. Chiu, P. S. Chang, Y. C. Chou, W. H. Chang, *ACS Nano* **2014**, *8*, 2951.
[20] X. Zhou, J. Cheng, Y. Zhou, T. Cao, H. Hong, Z. Liao, S. Wu, H. Peng, K. Liu, D. Yu, *J. Am. Chem. Soc.* **2015**, *137*, 7994.
[21] G. Wang, X. Marie, I. Gerber, T. Amand, D. Lagarde, L. Bouet, M. Vidal, A. Balocchi, B. Urbaszek, *Phys. Rev. Lett.* **2015**, *114*, 097403.
[22] J. Shi, P. Yu, F. Liu, P. He, R. Wang, L. Qin, J. Zhou, X. Li, J. Zhou, X. Sui, S. Zhang, Y. Zhang, Q. Zhang, T. C. Sum, X. Qiu, Z. Liu, X. Liu, *Adv. Mater.* **2017**, *29*, 1701486.
[23] R. W. Boyd, *Nonlinear Optics*, Academic Press, New York **2020**.
[24] Y. R. Shen, *The Principles of Nonlinear Optics*, Wiley-Interscience, New York **2003**.
[25] W. Jie, X. Chen, D. Li, L. Xie, Y. Y. Hui, S. P. Lau, X. Cui, J. Hao, *Angew. Chem.* **2015**, *54*, 1185.

[26] N. Leisgang, J. G. Roch, G. Froehlicher, M. Hamer, D. Terry, R. Gorbachev, R. J. Warburton, *AIP Adv.* **2018**, *8*, 105120.
[27] W. Li, J. Li, *Nano Res.* **2015**, *8*, 3796.
[28] C. Cui, F. Xue, W.-J. Hu, L.-J. Li, *npj 2D Mater. Appl.* **2018**, *2*, 18.
[29] M. Dai, H. Chen, F. Wang, Y. Hu, S. Wei, J. Zhang, Z. Wang, T. Zhai, P. Hu, *ACS Nano* **2019**, *13*, 7291.
[30] S. Jandl, C. Carlone, *Solid State Commun.* **1978**, *25*, 5.
[31] S. Lei, F. Wen, L. Ge, S. Najmaei, A. George, Y. Gong, W. Gao, Z. Jin, B. Li, J. Lou, J. Kono, R. Vajtai, P. Ajayan, N. J. Halas, *Nano Lett.* **2015**, *15*, 3048.
[32] Z. Chen, K. Gacem, M. Boukhicha, J. Biscaras, A. Shukla, *Nanotechnology* **2013**, *24*, 415708.
[33] Y. Zhang, D. Huang, Y. Shan, T. Jiang, Z. Zhang, K. Liu, L. Shi, J. Cheng, J. E. Sipe, W. T. Liu, S. Wu, *Phys. Rev. Lett.* **2019**, *122*, 047401.